# Wind and Solar Power Integration in Electricity Markets and Distribution Networks Through Service-Centric Virtual Power Plants

Despina Koraki and Kai Strunz

***Abstract*—A virtual power plant (VPP) is formulated and developed as a service-centric aggregator that enables the market integration of distributed energy resources and simultaneously supports cooperation with the distribution system operator in addressing the issue of network usage. A suitable schedule of interactions and communications between aggregators, market operators, system operators, generators, and consumers, regarding electricity market participation and network operation is proposed and presented in a sequence diagram. The cooperation on congestion management in the distribution network is highlighted as a solution to relieve network constraints via the optimal adjustment of active and reactive power of VPP resources while maximizing renewable energy integration across the pool under management. The VPP reduces uncertainty affiliated with input data by employing the latest forecasts through a rolling horizon approach in the planning stage. Thanks to the flexibility of the VPP to perform rescheduling in accordance with agreements it negotiated with its resources, it becomes possible to refrain from undesirable curtailments. Both the market-integrative and the service-centric roles of the VPP are verified through modeling and simulation with a benchmark European distribution network. The results confirm the added value of the proposed VPP in enhancing the integration of wind and solar power.**

***Index Terms*—Aggregator, congestion management, distribution network, electricity market, flexibility market, renewable energy, rolling horizon, solar power, virtual power plant, wind power.**

## NOMENCLATURE

*Abbreviations and Acronyms*

| | |
|---|---|
| Alt | Alternative. |
| CHP | Combined heat and power. |
| DER | Distributed energy resources. |
| DSO | Distribution system operator. |
| EV | Electric vehicle. |
| HV | High voltage. |
| LV | Low voltage. |
| MV | Medium voltage. |
| Opt | Option. |
| PV | Photovoltaic. |
| RES | Renewable energy sources. |
| TSO | Transmission system operator. |
| VPP | Virtual power plant or power pool. |

*Variables*

| | |
|---|---|
| $a_{\mathrm{P},mn,i}$, $a_{\mathrm{Q},mn,i}$ | Sensitivities relating change of branch $m$-$n$ flows to nodal injection changes of active and reactive power at nodes $i$ with VPP resources. |
| $\boldsymbol{\alpha}_{mn}^{\mathsf{T}}$ | Row vector of sensitivities relating change of branch $m$-$n$ flows to nodal injection changes of active and reactive power in network. |
| $b_{mn}$ | Susceptance of branch $m$-$n$. |
| $C_{\mathrm{f,chp}}$ | Fuel cost of CHP during interval $\tau$. |
| $c_{\mathrm{m,da}}$ | Forecasted day-ahead market price per amount of energy. |
| $c_{\mathrm{NG}}$ | Natural gas price per amount of energy. |
| $C_{\mathrm{op,e,sto}}$ | Operational cost of electrical storage unit during interval $\tau$. |
| $c_{\mathrm{op,e,sto}}$ | Average operational cost of electrical storage unit per amount of energy. |
| $C_{\mathrm{pen,imb}}$ | Penalty cost for intraday imbalances. |
| $E_{\mathrm{e,sto}}$ | Energy level of electrical storage unit. |
| $E_{\mathrm{e,sto0}}$ | Initial energy level of electrical storage unit. |
| $E_{\mathrm{e,sto,max}}$ | Maximum energy level of electrical storage unit. |
| $E_{\mathrm{e,sto,min}}$ | Minimum energy level of electrical storage unit. |
| $E_{\mathrm{th,sto}}$ | Energy level of thermal storage unit. |
| $E_{\mathrm{th,sto0}}$ | Initial energy level of thermal storage unit. |
| $E_{\mathrm{th,sto,max}}$ | Maximum energy level of thermal storage unit. |
| $E_{\mathrm{th,sto,min}}$ | Minimum energy level of thermal storage unit. |
| $g_{mn}$ | Conductance of branch $m$-$n$. |
| $H_{\mathrm{a}}$ | Anticipation horizon. |
| $H_{\mathrm{b}}$ | Bid horizon. |
| $H_{\mathrm{da}}$ | Day-ahead planning horizon. |
| $H_{\mathrm{id}}$ | Intraday scheduling horizon. |
| $i$ | Integer counter. |
| $I$ | Number of VPP resources on network. |
| $\boldsymbol{J}_{PQ,\theta V}$ | Power flow Jacobian matrix. |
| $\boldsymbol{J}_{\theta V,PQ}$ | Power flow Inverse Jacobian matrix. |
| $k$ | Integer counter. |
| $N_{\mathrm{chp}}$, $N_{\mathrm{e,sto}}$, $N_{\mathrm{th,sto}}$ | Number of CHP and electrical and thermal storage units. |
| $N_s$ | Number of scenarios of day-ahead renewable power generation forecasts. |
| $P_{\mathrm{e,chp}}$ | Electrical power injection of CHP unit. |

Manuscript received August 23, 2016; revised January 15, 2017 and April 19, 2017; accepted May 20, 2017. Date of publication June 1, 2017; date of current version December 20, 2017. This work was supported by the EU FP7 Project SUSTAINABLE (no. 308755) and the Project OptNetzE (no. 0325814A), funded by the Federal Ministry for Economic Affairs and Energy (BMWi). Paper no. TPWRS-01286-2016. *(Corresponding author: Despina Koraki.)*

The authors are with the Chair of Sustainable Electric Networks and Sources of Energy, School of Electrical Engineering and Computer Science, Technische Universität Berlin, Berlin 10623, Germany (e-mail: despoina.koraki@tu-berlin.de; kai.strunz@tu-berlin.de).

Digital Object Identifier 10.1109/TPWRS.2017.2710481

| | |
|---|---|
| $P_{\mathrm{e,chp,max}}$, $P_{\mathrm{e,chp,min}}$ | Maximum and minimum electrical power injection of CHP unit. |
| $P_{\mathrm{e,l}}$, $P_{\mathrm{th,l}}$ | Total electrical and thermal loads in VPP. |
| $P_{\mathrm{e,sto}}$ | Electrical power injection of storage unit. |
| $pf$ | Penalty factor in EUR/MWh. |
| $P_{\mathrm{f},mn}$ | Active power flow from node $m$ to $n$. |
| $P_{\mathrm{fmax},mn}$ | Maximum active power transfer capability of branch $m$-$n$, at a given power factor. |
| $P_i$ | Active power injection at node $i$. |
| $P_{\mathrm{imb,id}}$ | Active power imbalance exchanged toward intraday energy market. |
| $P_{\mathrm{m,da}}$ | Active power exchanged toward day-ahead energy market. |
| $P_{\mathrm{res}}$ | Electrical power injection of renewable energy sources. |
| $P_{\mathrm{th,chp}}$ | Thermal power injection of CHP unit. |
| $P_{\mathrm{th,sto}}$ | Thermal power injection of storage unit. |
| $p_s$ | Probability of occurrence for each scenario $s$. |
| $Q_i$ | Reactive power injection at node $i$. |
| $reconf$ | Boolean that indicates if network has been reconfigured or not. |
| $s$ | Counter of day-ahead renewable power generation forecast scenarios. |
| $t_{\mathrm{a}}$ | Actual time. |
| $t_{\mathrm{h}}$ | Horizon time. |
| $T_{\mathrm{m}}$ | Intraday market processing interval. |
| $V_i$ | Voltage at node $i$. |
| $\Delta$ | Difference operator. |
| $\eta_{e,\mathrm{ch}}$, $\eta_{e,\mathrm{dis}}$ | Charging and discharging efficiency of electrical storage unit. |
| $\eta_{\mathrm{th,ch}}$, $\eta_{\mathrm{th,dis}}$ | Charging and discharging efficiency of thermal storage unit. |
| $\eta_{\mathrm{chp}}$ | Electrical efficiency of CHP unit. |
| $\theta_i$ | Voltage angle at node $i$. |
| $\lambda_{\mathrm{chp}}$ | Heat to electrical power ratio of CHP unit. |
| $\tau$ | Time step size. |
| $\tau_{\mathrm{da}}$ | Day-ahead time step size. |
| $\tau_{\mathrm{id}}$ | Intraday time step size. |
| $\varphi_i$ | Phase angle between voltage and current at node $i$. |

## I. Introduction

THE share of wind and solar power in electricity grids has rapidly increased in the last years, with a main driver being the reduction of green house gas emissions. A number of governments have developed incentives to facilitate the integration of renewable energy sources (RES). In Germany, for example, the large-scale integration of RES has been supported by the German Renewable Energy Sources Act through which feed-in tariffs for wind and solar energy were introduced. Moreover, a revision of the Renewable Energy Sources Act in 2014 suggested the direct marketing of RES [1]. According to this mechanism, the RES owners can directly participate in the energy market and receive a market premium. The premium covers the revenue difference between the market clearing price and the subsidized feed-in tariff. It so reduces the financial risks for the RES owners. However, there is a power limit for the participation in the direct marketing scheme. This lower limit is 500 kW for the units that are commissioned to be installed by 2016 and 100 kW for the following installations. Furthermore, for the participation in the German day-ahead energy market, there is a minimum increment of 100 kW for each hour. The aggregation of multiple RES plays, therefore, an important role in enabling their market participation [2].

Virtual power plants respectively pools (VPPs) serve as aggregators of distributed energy resources (DER), including RES, storage, controllable loads, and electric vehicles (EVs) to support their market integration. Prior research was mainly concerned with the optimal dispatching of the resources within a VPP to participate in energy markets. In [3] the bidding strategy of a VPP participating in a joint energy and reserve market was presented. In [4] the bidding strategy of an EV aggregator that participates in both day-ahead and reserve markets was developed, and the compensation of the EV owners for the battery degradation was included. A model that also includes thermal loads and storage was introduced in [5]. Uncertainties in the generation and load profiles, in the energy market prices and in the bids of other market participants were considered for the day-ahead energy market bidding of VPPs in [6]. A VPP for sequential bidding in day-ahead and real-time markets was developed in [7]. The impact on a VPP's profit of participating in spinning reserve markets and considering different risk levels for real-time imbalances was assessed in [8]. Issues of demand side management within a VPP were dealt with in [9], [10].

Another critical aspect of the large-scale integration of RES is, however, the security of networks. The VPPs in [11] and [12] deal with voltage regulation and over-frequency problems. Network security can also be threatened through overloadings of transformers and feeders. To deal with the loading of feeders, especially in distribution networks, congestion management has become an imminent need. In Germany, for example, the curtailment of RES connected to distribution networks has risen dramatically [13] due to congestions. In prior research, distribution network congestion management focused on cases in which congestion is caused due to new types of loads, such as EVs, connected to LV feeders. In [14], an EV charging method was developed to take into consideration the network constraints, and in [15] the introduction of a distribution network capacity market with shadow prices for congested areas was suggested.

The issue of network security is further complicated by the uncertainty inherent with renewable power generation. This uncertainty must be dealt with at different time scales depending on whether short-term or long-term decisions are to be made. The issue was addressed in [16] through a two-stage distribution system management, covering the actions of the DSO at different time horizons. In the first stage, the day-ahead actions of the DSO are planned. In the second stage, the planning shifts to the intraday actions. The scheduling of the second stage is performed taking into consideration the results of the first stage and, in addition to that, updated intraday forecasts. Those actions are performed during the day on a rolling basis of four hours ahead to minimize forecast deviations. Rolling horizon

approaches have also been applied to renewable power integration in [17], [18], [19].

The work performed here takes into consideration the uncertainty of renewable power generation and fully acknowledges the key importance of both the market integration of DER and a secure network operation. This is achieved thanks to novel VPP functions proposed here. In the design of the service-centric VPP, a competitive electricity market environment where a uniform marginal price is defined is assumed. Such a situation is common in Europe and encountered in Germany for example. Here, congestion is not dealt with by locational marginal pricing. The first key contribution of this work lies in the formulation of a service-centric methodology and cooperation of the VPP and the distribution system operator (DSO). This service-centric VPP encompasses both the market integration of DER and the network security with the provision of the service of congestion relief. For the provision of this service, the VPP optimally readjusts the schedules of its resources. A service-centric VPP may also cover other ancillary services such as the support of voltage control and frequency control. The second important contribution lies in the definition and distinction of the roles of the participants and the required information exchange. It is shown, therefore, how the main actors for network operation, aggregation, and market operation can effectively cooperate for distribution network congestion management, while reducing the impact of uncertainty affiliated with renewable power generation through a rolling horizon method.

The framework for the cooperation and coordination between all the actors is described through a sequence diagram, which is given in Section II. The development of the algorithm, addressing the issue of congestion through the service of a VPP to the DSO, is described in Section III. The value of the proposed operation is substantiated through a case study in Section IV, where the CIGRE benchmark for distribution networks is employed [20]. A comparison between the suggested solution and the existing approach of RES curtailment is also performed. Conclusions are drawn in Section V.

## II. Coordinated Day-ahead and Intraday Operation Sequence

The DSO is responsible for the monitoring and the secure operation of the distribution network. As described in Section I, DSOs may curtail renewable power generation if network congestions cannot be relieved through network-related measures, such as reconfiguration. At the transmission grid level, TSOs of Germany deal with congestion through the so-called redispatching. According to this mechanism, the TSO can request generation units to readjust their schedule in order to prevent or mitigate congestion. Redispatching is also an option at the distribution network level. This is where the proposed actions of the VPP can come in, taking into account its opportunity to negotiate on behalf of a pool of DER. As such, the scale effects of the pool can be leveraged to offer services to the DSO.

For a better insight into the developed method and the general context, the coordinated actions of the key actors for the market operation, network operation, and aggregation are illustrated in the sequence diagram depicted in Fig. 1. This diagram describes the proposed day-ahead and intraday operation sequence, including the novel VPP service.

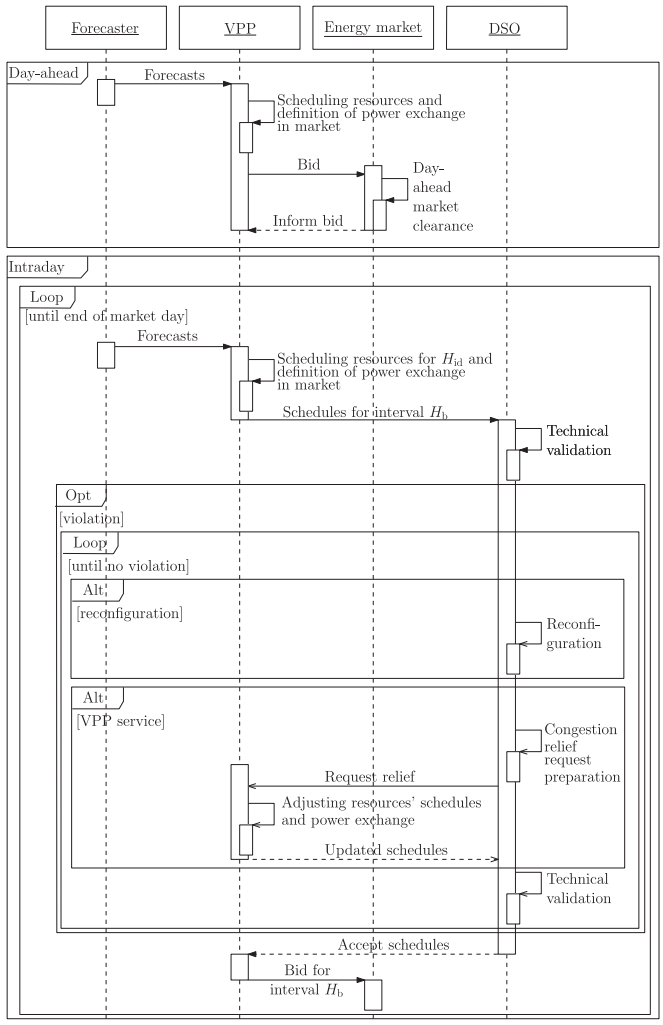


Fig. 1. Sequence diagram for the day-ahead and intraday operation.

In the day-ahead planning, the uncertainties of renewable power generation are modeled by different scenarios of renewable power forecasts. After the day-ahead operation has been planned, the intraday operations are scheduled just in time for market clearing. The bids are sent to apply for a bid horizon interval $H_{\mathrm{b}}$. This process is repeated successively for further intervals of $H_{\mathrm{b}}$. By successively scheduling resources just in time, the VPP benefits from updated rolling forecasts as an accurate input to supplement the information from the day-ahead planning. According to this rolling horizon approach, the most recent information on the market and the renewable power generation forecast is always available and utilized. The uncertainties of renewable power generation are, therefore, largely reduced. The actions of all the actors within the different time horizons are described in detail hereafter.

As shown in Fig. 1, the day-ahead operation begins with the transfer of information on renewable power generation forecasts and day-ahead energy market price forecasts to the VPP.

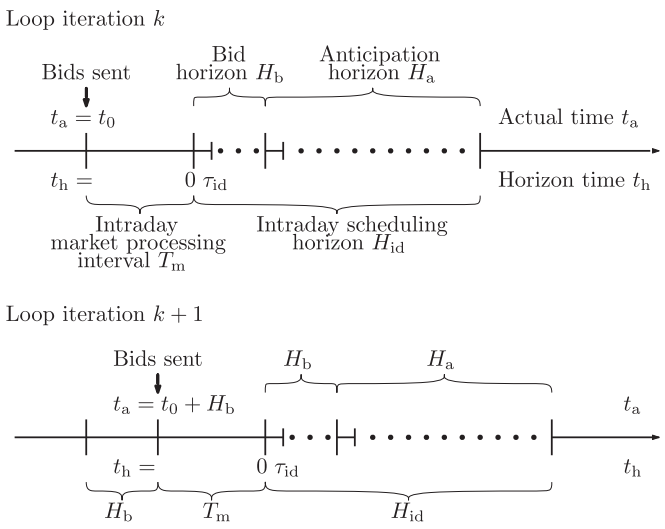


Fig. 2. Intraday rolling horizon method for scheduling.

The VPP prepares a schedule for the next day in accordance with these forecasts, the contracts the VPP has in place with its resources, and the technical characteristics of each DER. The involved dispatching is done stochastically, taking into consideration different scenarios for the wind and solar power generation. In this way, the uncertainty of renewables in the day-ahead planning is considered. Once the desired power exchange via the day-ahead energy market is defined, the bids are forwarded. The day-ahead energy market receives the bids from all the participants, and the auction takes place. Based on all bids received, the market is cleared and the participants are informed.

The actions of the intraday operation are performed in a loop, one iteration of which is shown in Fig. 1. At the end of each iteration, the VPP sends its bid applicable for bid horizon interval $H_\mathrm{b}$ to the market. Even though this bid applies to $H_\mathrm{b}$, the internal intraday scheduling horizon of the VPP goes beyond that. In Fig. 2, the latter is illustrated through $H_\mathrm{id}$, which extends the bid horizon interval $H_\mathrm{b}$ by an interval $H_\mathrm{a}$ to anticipate upcoming bids for later iterations and to account for the inter-temporal characteristics of units such as storage. Even though the VPP would strive to send the bids as late as possible, it cannot do so later than an actual time instant $t_\mathrm{a} = t_0$ specified by market rules to allow for a sufficient time span of $T_\mathrm{m}$ for intraday market processing. For the scheduling, the VPP uses a horizon time counter $t_\mathrm{h}$. The latter is initialized to zero to start the scheduling of the resources as a key action at the beginning of a loop iteration, as described in Fig. 1. At the core of the scheduling process is the calculation of various costs that are computed at discrete time steps of $\tau_\mathrm{id}$ with the objective of minimizing overall cost over the intraday scheduling horizon $H_\mathrm{id}$. The underlying mathematical formulation is detailed in Section III. Once the VPP has completed the scheduling stage, it sends the results for interval $H_\mathrm{b}$ to the DSO for technical validation, also shown in Fig. 1.

The technical validation of the DSO consists of a power flow calculation with security analysis to verify whether the schedules violate the system constraints, such as line thermal limits. If a branch overload is detected, the DSO first attempts to resolve the congestion by modifying the network's configuration. If the reconfiguration mitigates the violation, this point of the technical validation is completed. However, if the reconfiguration does not relieve the congestion sufficiently or if a congestion at another branch is created, the DSO consults alternatives. At this point, a common approach that would be followed is the imposed curtailment of power injection. The alternative proposed in this work is a solution based on agreement.

The targeted provision of flexibility to support network security may be the result of a successful bid in a flexibility market or come from a bilateral agreement between the VPP and the DSO. This support can be provided by the VPP through the optimal readjustment of the schedules of its resources, including those that impact the power flows on the congested branches. For the activation of this service, the DSO communicates with the VPP and requests a relief service. The VPP then adjusts the schedules of its resources taking care of constraints, which are further explained in Section III.

The DSO obtains the updated schedules of the VPP and performs a new technical validation. If the new schedules are accepted, the VPP is informed. As a final step, the VPP bids into the intraday market for the interval $H_\mathrm{b}$ as the final step of this iteration. As mentioned above, the bids must be sent by actual time $t_\mathrm{a} = t_0$.

In the next iteration, the process is repeated to perform the scheduling for the next intraday horizon interval. Again, the VPP takes into account the latest forecasts in the scheduling over a rolling horizon covering an interval for the bids and a further interval in anticipation of bidding in the next iteration. The distinctive character of the rolling horizon methodology is illustrated in Fig. 2 through the shifting of the intraday scheduling horizon along the actual time axis when transitioning from loop iterations $k$ to $k+1$.

## III. Service-Centric Operation

The service-centric feature of the VPP reflects its priority in developing services that are of value to diverse actors involved in the energy and power system. In this section, the services of facilitating market integration and offering congestion relief are detailed. Further ancillary services may be added accordingly. The market integration of resources by the VPP in the day-ahead and intraday markets is described in Section III-A. Having provided the details for the scheduling of the resources of the VPP in the aforementioned section, the readjustment of the resource outputs for the realization of the congestion relief service is presented in Section III-B. This service to the DSO is depicted through a flowchart, and each actor's operations are analyzed.

### A. Energy Market Participation Service to Resources

The VPP seeks to attract a diverse pool of resources as subscribers in order to offer appropriate power balancing and opportunities of market participation. These opportunities are important for small DER that cannot directly participate in the energy markets. Furthermore, being part of a VPP, consumers

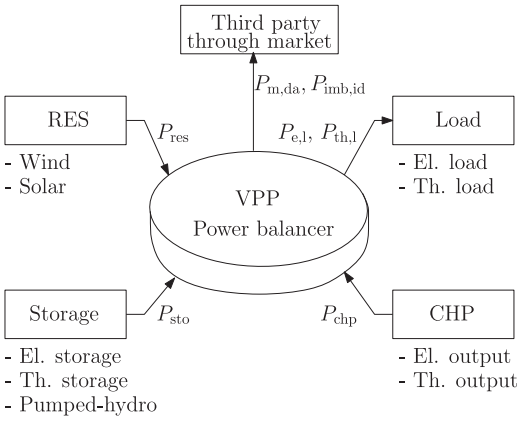


Fig. 3. Power transactions and conventions within the VPP.

or producers have the opportunity to obtain variable tariffs based on their characteristics and preferences. As described in Section I, it is assumed that the modeled VPP participates in an electricity market environment with a uniform marginal price, as the one of Germany. In this environment, the system operators are responsible to procure energy to cover grid losses.

The power transactions and balancing within the modeled VPP are shown in Fig. 3. The resources include RES, combined heat and power (CHP) units, storage, and loads. RES are wind and solar power generators. Furthermore, both the electrical and thermal outputs of CHP units are considered for the power balance. Storage covers electrical and thermal, as well as small pumped-hydro storage. The VPP is responsible for the power balance in both the day-ahead and intraday operations.

For the participation of the VPP in the day-ahead market, the forecasts of renewable power generation are an important input. These forecasts may be obtained by an external forecaster, as shown in Fig. 1, and include the forecasts for all the 24 hours of the following day in time step sizes of $\tau_{\mathrm{da}}$. As it was mentioned in Section II, day-ahead forecasts of renewable power generation include uncertainties. These uncertainties in the day-ahead operation are modeled by different renewable power generation forecast scenarios [21] over a day-ahead planning horizon $H_{\mathrm{da}}$. In particular, scenarios of renewable power generation forecasts are generated and then reduced to a total number of $N_s$, with each scenario $s$ being characterized by a probability of $p_s$. In order to consider the uncertainty of renewable power generation in the VPP, it must be possible to maintain the power balance for every forecast scenario. The electrical and thermal power balance equations of the day-ahead operation for each scenario $s$ and for each $t_{\mathrm{h}}$ within the day-ahead planning horizon $H_{\mathrm{da}}$ are formulated as follows:

$$\sum_{i=1}^{N_{\mathrm{chp}}} P_{\mathrm{e,chp},i,s}(t_{\mathrm{h}}) + \sum_{i=1}^{N_{\mathrm{e,sto}}} P_{\mathrm{e,sto},i,s}(t_{\mathrm{h}}) + P_{\mathrm{res},s}(t_{\mathrm{h}}) - P_{\mathrm{m,da}}(t_{\mathrm{h}}) = P_{\mathrm{e,l}}(t_{\mathrm{h}}) \quad (1)$$

$$\sum_{i=1}^{N_{\mathrm{chp}}} P_{\mathrm{th,chp},i,s}(t_{\mathrm{h}}) + \sum_{i=1}^{N_{\mathrm{th,sto}}} P_{\mathrm{th,sto},i,s}(t_{\mathrm{h}}) = P_{\mathrm{th,l}}(t_{\mathrm{h}}) \quad (2)$$

According to (1), the electrical power injection of the CHP units, the storage units, the renewable power generation, and minus the power that is output to the day-ahead market is to be equal to the electrical load in the VPP. In the same context, in (2) the thermal power that is generated by the CHP units and the thermal power output of the thermal storage units is to equal the VPP's thermal load. The power that is exchanged in the day-ahead market as well as the electrical and thermal loads are not functions of individual forecast scenarios.

The resources are scheduled for the time horizon $H_{\mathrm{da}}$ with a time step size $\tau_{\mathrm{da}}$ according to power balance constraints (1), (2), the units' constraints (11), (14), (15), (17), (18) given in Appendix A, the forecasted day-ahead market prices, and the renewable power generation forecast scenarios. The objective of the dispatching is to minimize the VPP's operational cost. The operational costs of the RES are comparatively low and are therefore neglected, as in [6]. The objective function for the day-ahead market involvement is thus formulated with the CHP fuel cost, the operational cost of storage, the forecasted day-ahead market price for energy, and the scenario probabilities $p_s$:

$$\min \sum_{s=1}^{N_s} p_s \left( \sum_{t_{\mathrm{h}}=1\tau_{\mathrm{da}}}^{H_{\mathrm{da}}} \left( \sum_{i=1}^{N_{\mathrm{chp}}} C_{\mathrm{f,chp},i,s}(t_{\mathrm{h}}) + \sum_{i=1}^{N_{\mathrm{e,sto}}} C_{\mathrm{op,e,sto},i,s}(t_{\mathrm{h}}) - P_{\mathrm{m,da}}(t_{\mathrm{h}}) c_{\mathrm{m,da}}(t_{\mathrm{h}}) \tau_{\mathrm{da}} \right) \right) \quad (3)$$

which is subject to constraints (1), (2), (11), (14), (15), (17), and (18).

After the day-ahead market clearance, the intraday operation is planned according to the rolling horizon methodology described in Section II. The electrical and the thermal power balance equations for each $t_{\mathrm{h}}$ within the intraday scheduling horizon $H_{\mathrm{id}}$ illustrated in Fig. 2 are the following:

$$\sum_{i=1}^{N_{\mathrm{chp}}} P_{\mathrm{e,chp},i}(t_{\mathrm{h}}) + \sum_{i=1}^{N_{\mathrm{e,sto}}} P_{\mathrm{e,sto},i}(t_{\mathrm{h}}) + P_{\mathrm{res}}(t_{\mathrm{h}}) - P_{\mathrm{m,da}}(t_{\mathrm{h}}) - P_{\mathrm{imb,id}}(t_{\mathrm{h}}) = P_{\mathrm{e,l}}(t_{\mathrm{h}}) \quad (4)$$

$$\sum_{i=1}^{N_{\mathrm{chp}}} P_{\mathrm{th,chp},i}(t_{\mathrm{h}}) + \sum_{i=1}^{N_{\mathrm{th,sto}}} P_{\mathrm{th,sto},i}(t_{\mathrm{h}}) = P_{\mathrm{th,l}}(t_{\mathrm{h}}) \quad (5)$$

According to (4), the intraday electrical power balance is to be maintained taking into consideration the power exchanged in the day-ahead market and the updated intraday forecasts. The thermal power balance (5) also has to be maintained. In the intraday planning, the purpose of the VPP is to deliver the day-ahead market power exchanges and to internally cover imbalances due to the updated renewable power generation forecasts. If it is not possible to cover the imbalances within its pool, then the VPP exchanges the active power $P_{\mathrm{imb,id}}(t_{\mathrm{h}})$ in the intraday market. The dispatching of the resources of the VPP is, therefore, performed with the target of minimizing the active power imbalance $P_{\mathrm{imb,id}}(t_{\mathrm{h}})$ that is exchanged in the intraday market. This is accomplished by considering a penalty cost $C_{\mathrm{pen,imb}}(t_{\mathrm{h}})$ for the exchanged imbalance during the optimization of the resources'

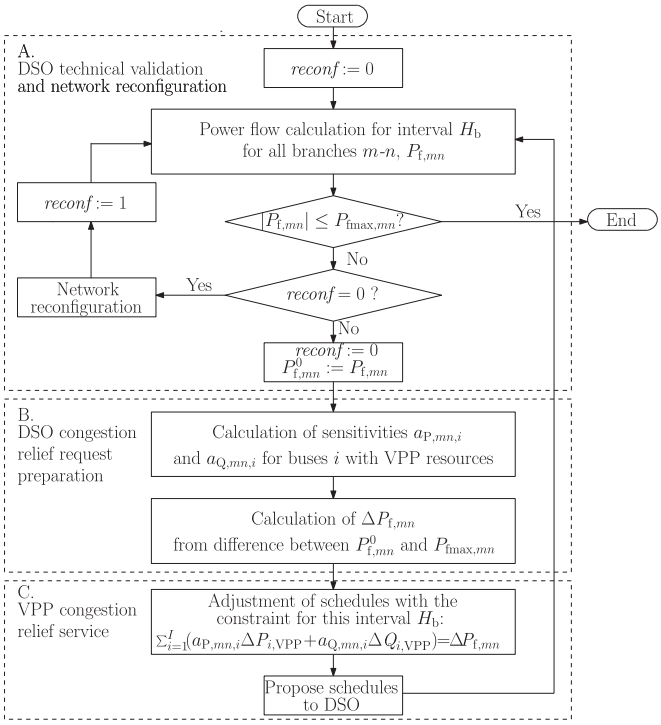


Fig. 4. Flowchart for technical validation and congestion management.

schedules. The objective function also covers the CHP fuel cost and the operational cost of storage:

$$\min \sum_{t_\mathrm{h}=1}^{H_\mathrm{id}} \tau_\mathrm{id} \left( \sum_{i=1}^{N_\mathrm{chp}} C_{\mathrm{f,chp},i}(t_\mathrm{h}) + \sum_{i=1}^{N_\mathrm{e,sto}} C_{\mathrm{op,e,sto},i}(t_\mathrm{h}) + C_\mathrm{pen,imb}(t_\mathrm{h}) \right) \quad (6)$$

The optimization is performed for the time horizon $H_\mathrm{id}$ with a time step size $\tau_\mathrm{id}$ and according to the power balance constraints (4) and (5), the units' constraints (11), (14), (15), (17), (18) given in Appendix A, and the updated intraday renewable power generation forecasts. Details on the modeling of all the VPP's units and the minimization of the exchanged intraday imbalances are included in Appendix A.

### *B. Congestion Relief Service to DSO*

Dedicated flexibility markets or direct agreements between VPP and DSO offer novel opportunities for the provision of system services, as introduced in Section II. This coordinated operation and the steps followed for the provision of the congestion relief service are shown in the flowchart of Fig. 4. The flowchart is decomposed into three parts to emphasize the most important actions of the two actors.

The actions illustrated in the flowchart are part of the actions of the DSO and the VPP shown in the intraday operation of Fig. 1. In particular, the starting point of the flowchart is the point at which the DSO receives the VPP's schedules for a time interval of $H_\mathrm{b}$. Part A of the flowchart covers the technical validation of the DSO and the first alternative that is being explored in case of a violation such as congestion. This alternative encompasses network reconfiguration. If the congestion was not relieved by the first alternative, the second alternative is explored. The second alternative is the VPP's service for congestion relief. The DSO's preparatory actions for requesting the congestion relief service are included in part B of the flowchart. This includes the preparation of the information to be sent from the DSO to the VPP to request the service. Part C illustrates the provision of the congestion relief service by the VPP. This covers the optimal adjustment of the schedules of the resources of the VPP and the proposal of the updated schedules to the DSO. The termination point of the flowchart is the point at which the DSO informs the VPP about the possible acceptance of the schedules. The three parts of the flowchart are described in detail below.

Part A is concerned with the DSO's technical validation and network reconfiguration. The two main functions of this part are the power flow calculation and the network reconfiguration in the case of a congestion. Both functions consider all the network's branches and refer to a specific time interval of $H_\mathrm{b}$ for which the power flow calculation takes place. If the magnitude of the power flow $P_{\mathrm{f},mn}$ is smaller than the maximum active power transfer capability $P_{\mathrm{fmax},mn}$, which relates to the maximum apparent power at a given power factor, then the schedules of the VPP are accepted. The VPP is then informed.

If the magnitude of the power flow is larger than $P_{\mathrm{fmax},mn}$, then the branch is overloaded. The DSO then explores the first mitigation alternative, which is network reconfiguration to resolve the issue. This takes place if the network has not been reconfigured for this time interval as indicated by the value of the variable $reconf$. Upon the DSO's attempt, the value 1 is assigned to $reconf$, and the power flow calculation is repeated. If, however, the reconfiguration creates a branch overload at another branch or if the congestion is not fully relieved, another alternative is to be explored.

The complement to the DSO's action of reconfiguration of part A is the request for a congestion relief service by the VPP. The preparation of the DSO's request is given in part B of the flowchart of Fig. 4. For the activation of this service, the DSO carries out the relevant preparatory calculations. At first, the sensitivities of the active power flow on branch $m$-$n$ to changes of active and reactive power injections from the resources of the VPP at nodes $i$ are calculated. These sensitivities for each node $i$ are denoted by $a_{\mathrm{P},mn,i}$ and $a_{\mathrm{Q},mn,i}$. Details on the calculation of these sensitivities are included in Appendix B. The second calculation of the DSO refers to the difference between the power flow value $P^0_{\mathrm{f},mn}$ that was calculated in part A and the limit $P_{\mathrm{fmax},mn}$. This difference is expressed by $\Delta P_{\mathrm{f},mn} = P_{\mathrm{fmax},mn} - P^0_{\mathrm{f},mn}$. The VPP should, therefore, modify the power flow over the congested branch from its resources by $\Delta P_{\mathrm{f},mn}$ to get it back to $P_{\mathrm{fmax},mn}$. The sensitivities $a_{\mathrm{P},mn,i}$ and $a_{\mathrm{Q},mn,i}$ for all the nodes $i$ with VPP resources and $\Delta P_{\mathrm{f},mn}$ are sent to the VPP to implement part C of the flowchart.

Part C of the flowchart covers the VPP's congestion relief service. Upon request of the DSO, the VPP adjusts the schedules of its resources taking into consideration an additional

constraint, hereafter called the flow change request constraint. This constraint is based on the calculations of part B and is given by:

$$\sum_{i=1}^{I}(a_{\mathrm{P},mn,i}\Delta P_{i,\mathrm{VPP}} + a_{\mathrm{Q},mn,i}\Delta Q_{i,\mathrm{VPP}}) = \Delta P_{\mathrm{f},mn} \quad (7)$$

According to (7), the sum of the changes of power injections of the VPP's resources weighted by the sensitivities is to equal $\Delta P_{\mathrm{f},mn}$. Based on the flow change request constraint (7), the contribution of the VPP's resources to the power flow over branch $m$-$n$ will be modified by the amount required to relieve the congestion. As a further constraint, the changes $\Delta P_{i,\mathrm{VPP}}$ and $\Delta Q_{i,\mathrm{VPP}}$ must be such that the values given by the rated power of the individual resources are not exceeded and voltage bands are not violated.

For the provision of the congestion relief service of part C, the optimization that was explained in (6) serves as the basis. The difference from what was described in Section III-A is as follows: Apart from the constraints (4), (5), (11), (14), (15), (17), and (18), the flow change request constraint (7) is also considered for the time interval of $H_{\mathrm{b}}$ in which technical validation takes place.

In the special case in which it is desired to maintain unchanged power factor angles for the provision of the congestion relief service, the flow change request constraint (7) can be modified. In particular, it can be expressed in terms of the sum of active power injection changes and is formulated as follows:

$$\sum_{i=1}^{I}(a_{\mathrm{P},mn,i} + a_{\mathrm{Q},mn,i}\tan\varphi_i)\Delta P_{i,\mathrm{VPP}} = \Delta P_{\mathrm{f},mn} \quad (8)$$

The new proposed schedules of the VPP are then sent to part A of the flowchart for the AC power flow calculation by the DSO. The cost for the adjustment of the schedules of the resources is included in the cost of the flexibility service and is covered by the bilateral agreement between the two actors. If the VPP's congestion relief service does not adequately mitigate the problem and if no other generation or load can be reduced, renewable power injection may be reduced as a last resort.

## IV. Case Study

In what follows the performance of the proposed service-centric operation of the VPP is validated and its value is put into evidence. It is shown how the VPP in cooperation with the DSO addresses emerging challenges of increased RES penetration through its novel congestion relief service. A day with high renewable power generation that would otherwise lead to network congestions is selected. The case study is structured as follows. In Section IV-A the input data are described. In Section IV-B the modeling of the uncertainties of renewable power generation is presented. Section IV-C includes the results of the market participation of the VPP. In Section IV-D, the congestion relief service is validated. In Section IV-E, a comparative analysis of a case without and with the congestion relief service of the VPP is included.

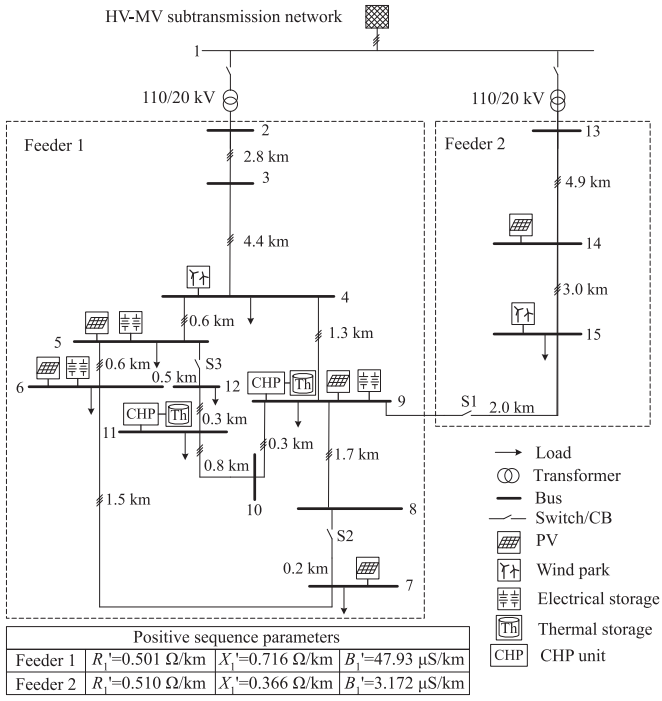


| Positive sequence parameters | | | |
|---|---|---|---|
| Feeder 1 | $R_1$'=0.501 Ω/km | $X_1$'=0.716 Ω/km | $B_1$'=47.93 μS/km |
| Feeder 2 | $R_1$'=0.510 Ω/km | $X_1$'=0.366 Ω/km | $B_1$'=3.172 μS/km |

Fig. 5. MV benchmark network of case study.

### A. Input Data

The simulation is performed on a representative European MV network from [20], and the network of the case study is shown in Fig. 5. The switches S1, S2, and S3 are normally open. The network is of radial structure, but may also be operated as a ring. The simulations were done in the MATLAB environment. For the VPP optimization, the Gurobi solver [22] was used. For the power flow calculations regarding the DSO operation, Matpower [23] was used. The day-ahead planning horizon selected is $H_{\mathrm{da}} = 24$ h and the intraday scheduling horizon selected is $H_{\mathrm{id}} = 4$ h. The day-ahead time step size $\tau_{\mathrm{da}}$ and the intraday time step size $\tau_{\mathrm{id}}$ are assumed to be 15 min. The bid horizon is selected to be $H_{\mathrm{b}} = 15$ min.

The units of the network of Fig. 5 as well as the number of households at each bus are listed in Table I. The units that are controlled by the VPP are also marked in the table. The power factor of 0.97 of the loads is also assigned to the electrical storage [20]. Apart from the controllable units of this particular network, the VPP also coordinates units of other locations. The total load and all units of the VPP of the case study are listed in Table II. The RES day-ahead and intraday power generation data and the market prices of the case study were selected for Germany, for a winter day of 2015 with high renewable power generation. More information on the data of the case study and the tables are included in Appendix C.

### B. Modeling of Renewable Power Generation Uncertainties

The modeling of the renewable power generation uncertainties for the day-ahead and intraday operation is presented. As described in Section III-A, the uncertainties of the day-ahead renewable power generation forecasts are modeled by scenar-

TABLE I
DATA OF NETWORK OF CASE STUDY

| Bus | Type of unit | Maximum power output (MW) | Member of VPP | Number of households |
|---|---|---|---|---|
| 4 | Wind park | 5 | no | 224 |
| 5 | PV | 0.53 | yes | 351 |
| | Electrical storage | 0.53 | yes | |
| 6 | PV | 0.88 | yes | 591 |
| | Electrical storage | 0.88 | yes | |
| 7 | PV | 0.67 | no | 445 |
| 9 | CHP | 1.5 | yes | 477 |
| | Thermal storage | 1.5 | yes | |
| | PV | 0.72 | yes | |
| | Electrical storage | 0.72 | yes | |
| 11 | CHP | 1.2 | yes | 386 |
| | Thermal storage | 1.2 | yes | |
| 14 | PV | 3.5 | no | – |
| 15 | Wind park | 5 | yes | 169 |

TABLE II
AGGREGATED DATA OF VPP OF CASE STUDY

| Type of unit | Maximum power (MW) |
|---|---|
| Wind power | 400 |
| PV | 280 |
| Electrical load | 280 |
| Thermal load | 225 |
| Electrical storage | 90 |
| Thermal storage | 135 |
| Pumped hydro storage | 23 |
| EVs | 15 |
| CHP | 135 |

ios. First, scenarios of aggregated wind and aggregated solar power generation forecasts were generated based on [24]. The method presented in [24] refers to wind power generation scenarios and was extended for scenarios of solar power generation accordingly. For the generation of the scenarios, the aggregated forecasted and measured wind and solar power generation data from the German TSO 50Hertz were used. These data were normalized to the aggregated installed wind and solar power generation capacity inside the VPP. Second, the generated scenarios were reduced and then combined to 16. The scenario reduction was performed using the concept of probability distance, as described in [21]. The most commonly used Kantorovich distance is used here. In the intraday operation, the intraday renewable power generation forecast uncertainty is modeled through an updated rolling forecast. It covers a time horizon of four hours and is updated every $H_{\mathrm{b}}$, as it was described in Section II.

The day-ahead combined aggregated wind and solar power generation forecast scenarios and the intraday renewable power generation forecast used as inputs for the VPP are shown in Fig. 6. The intraday renewable power generation forecasts of the units of the MV benchmark network used as input for the DSO's technical validation are shown in Fig. 7.

### C. Energy Market Participation

The participation of the VPP in the day-ahead market and the schedules of its resources are verified. In the day-ahead operation, the power exchanges of the VPP in the day-ahead market are first calculated as it was described in Section III-A. In particular, according to the information on the day-ahead combined aggregated wind and solar power generation forecasts, the objective function (3), and constraints (1), (2), (11), (14), (15), (17), and (18), the VPP stochastically schedules its resources and defines its power exchanges for the planning horizon $H_{\mathrm{da}}$ of 24 hours. The day-ahead power exchanges of the VPP along with the day-ahead electricity market prices are illustrated in Fig. 8.

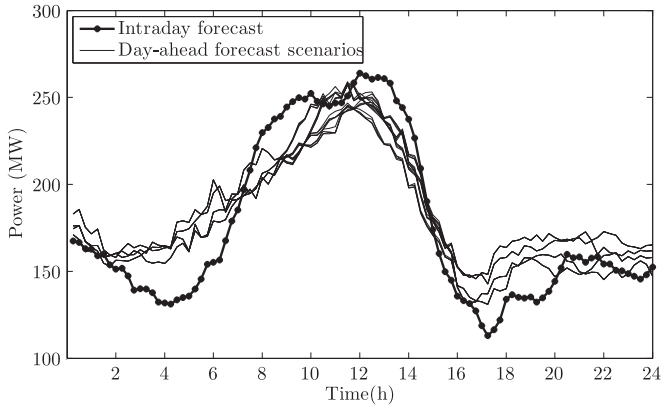


Fig. 6. Day-ahead and intraday renewable power generation forecasts.

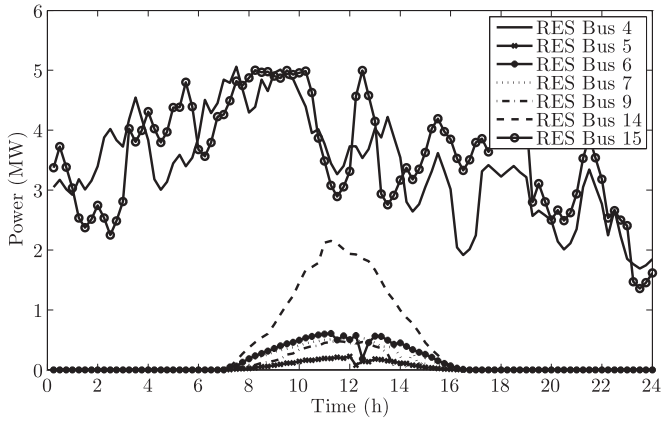


Fig. 7. Intraday wind and solar power generation forecasts at the nodes of the studied network.

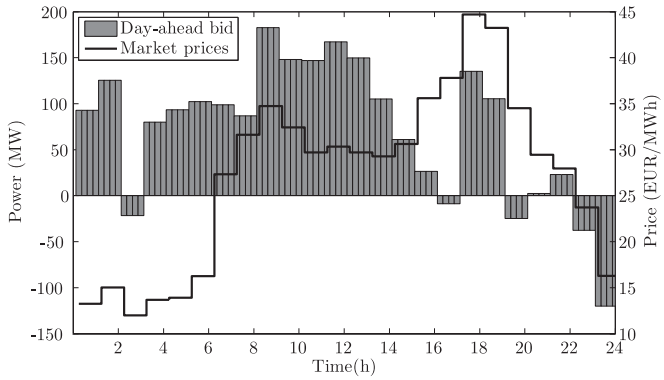


Fig. 8. Power traded by VPP in day-ahead market and market prices.

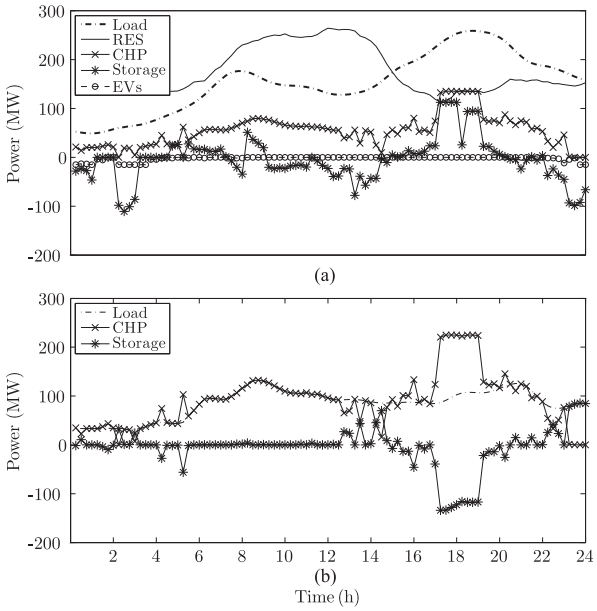


Fig. 9. VPP intraday optimal operation schedules for (a) electrical and (b) thermal power outputs.

In the intraday operation, the resources of the VPP are dispatched based on the objective function (6), the constraints (4), (5), (11), (14), (15), (17), and (18), and under consideration of the power exchanges in the day-ahead market. The intraday optimized schedules of the electrical and thermal resources of the VPP as well as the loads are illustrated in Fig. 9. According to Fig. 6, Fig. 8, and Fig. 9, the schedules of the resources of the VPP depend on the day-ahead market prices, the renewable power generation forecasts, and the load of the VPP at each time step. The VPP's resources generate more power during hours at which the market prices are expected to be high. In this way, the VPP's load is served, and the excess energy is sold in the market. The storage units charge during the hours at which the RES generation is larger than the demand and when the market prices are low as also seen in Fig. 9(a). On the contrary, if the prices are expected to be high, the electric storage units discharge to sell the previously stored energy in the market. The EVs charge at low electricity prices. Finally, the generation of the CHP units depends both on the prices and the thermal demand. The thermal power outputs of the CHP units, the thermal storage units, and of the thermal demand are shown in Fig. 9(b).

### *D. Congestion Relief Service*

In what follows it is illustrated how the VPP successfully mitigates congestion using the optimization of (6) with associated constraints. For the validation, the sequence of actions of the flowchart of Fig. 4 is followed. At the starting point of the flowchart, the DSO receives the schedules of the resources connected to the network. The power flow calculation is then performed by the DSO in part A. At 09:00 h, congestion on branches 3-2 and 4-3 is identified. The power flow over branch 4-3 is shown in Fig. 10 and the squares indicate the unconstrained solution, which is the power flow calculation result of

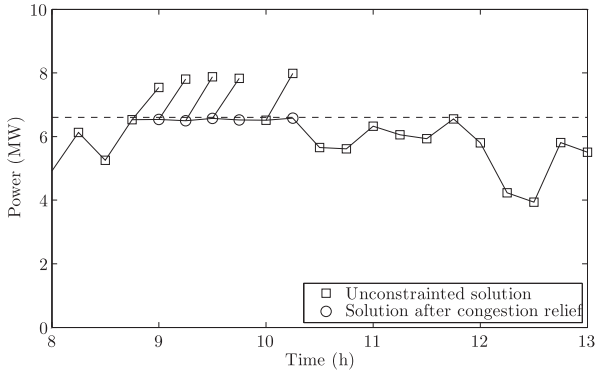


Fig. 10. Power flow over branch 4-3 in comparison to maximum power transfer capability. The power flow for the solution provided by the congestion relief service at 09:00 h, 09:15 h, 09:30 h, 09:45 h, and 10:15 h is marked with "o".

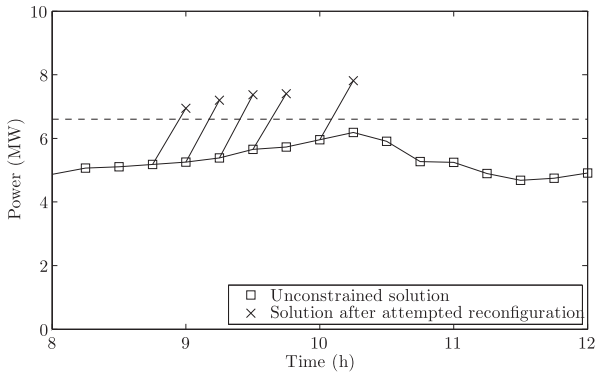


Fig. 11. Power flow over branch 14-13 in comparison to maximum power transfer capability. The power flow for the case of attempted reconfigurations at 09:00 h, 09:15 h, 09:30 h, 09:45 h, and 10:15 h is marked with "x".

TABLE III
SENSITIVITIES FOR BRANCHES 3-2 AND 4-3 AT 09:00 H

| Node $i$ | 5 | 6 | 9 | 11 |
|---|---|---|---|---|
| $a_{\mathrm{P},32,i}$ | 0.88 | 0.88 | 0.87 | 0.87 |
| $a_{\mathrm{Q},32,i}$ | 0.02 | 0.02 | 0.02 | 0.02 |
| $a_{\mathrm{P},43,i}$ | 0.93 | 0.93 | 0.92 | 0.92 |
| $a_{\mathrm{Q},43,i}$ | 0.01 | 0.01 | 0.01 | 0.01 |

part A without taking any action. To relieve the congestion, the DSO firstly attempts to reconfigure the network. To illustrate the attempted reconfiguration by the DSO, the power flow over branch 14-13 is shown in Fig. 11. The squares indicate again the unconstrained solution without taking any action. If the DSO reconfigures the network by closing switch S1, the maximum power transfer capability of branch 14-13 is exceeded. This happens because branch 14-13 is also highly loaded due to the power generation of the wind park that is located there. The result of the reconfiguration is indicated by the "x" at the time instant 09:00 h in Fig. 11.

An alternative to network reconfiguration is the congestion relief service of the proposed service-centric VPP. The DSO prepares, therefore, the request for the VPP's congestion relief service, as in part B of the flowchart of Fig. 4. The sensitivities that are calculated for branches 3-2 and 4-3 are given in Table III.

TABLE IV
POWER FLOW MODIFICATION FOR BRANCHES 3-2 AND 4-3 AT 09:00 H

| | $\Delta P_{\mathrm{f},32}$ | $\Delta P_{\mathrm{f},43}$ |
|---|---|---|
| Modification (MW) | $-0.8$ | $-1.0$ |

TABLE V
AVOIDED CURTAILMENT OF RENEWABLE POWER IN MV BENCHMARK NETWORK THANKS TO VPP

| | with cong. relief service (MW) | without cong. relief service (MW) |
|---|---|---|
| 09:00 h | 1.08 | 0 |
| 09:15 h | 1.41 | 0 |
| 09:30 h | 1.41 | 0 |
| 09:45 h | 1.41 | 0 |
| 10:15 h | 1.52 | 0 |

The values of the differences $\Delta P_{\mathrm{f},32}$, $\Delta P_{\mathrm{f},43}$ are included in Table IV. The contents of these two tables are sent to the VPP for use in part C. The VPP then adjusts its schedules, and the new schedules are sent back from part C to part A for the DSO, according to Fig. 4. In part A, the DSO again performs the power flow calculation for 09:00 h to check if the congestion is relieved. The new power flow calculation result for branch 4-3 for 09:00 h is indicated with an "o" in Fig. 10. As it can be seen, the service was successful. The congestion relief service of the VPP is again activated for time instants 09:15 h, 09:30 h, 09:45 h, and 10:15 h. As it is shown, all congestions are successfully mitigated.

### E. Comparative Analysis

The added value of the proposed novel VPP congestion relief service is put into evidence by comparison with the situation where the service is not available. As it was shown in Fig. 11, the network reconfiguration cannot solve the identified congestions on branches 3-2 and 4-3. If the congestion relief service by the VPP is not available, then the next step would be the imposed curtailment of renewable power generation. This is often done as a last resort to ensure network security in markets with a uniform marginal price of electrical energy. The service-centric VPP, however, offers the alternative of relieving the congestions on branches 3-2 and 4-3. The curtailment of renewable power generation is, therefore, avoided. The results of this comparative analysis are included in Table V. If the VPP does not provide the congestion relief service, the curtailment of renewable power generation is not avoided. If the congestion relief service is available, more clean renewable generation is available.

## V. CONCLUSION

The large-scale integration of wind and solar power generation relies both on a successful market integration and efficient access to the power grid. The proposed service-centric virtual power plant here plays a vital role thanks to the flexibility contained in its pool of diverse resources. On the one hand, it enables the participation of DER in the energy market through aggregation functions. On the other hand, it can adjust the schedules of its resources in accordance with distribution network constraints in cooperation with the distribution system operator. These features also reflected the focus of this work.

As a first contribution, the roles and interactions of the different market actors, including the service-centric VPP, were identified and defined. A rolling horizon method was developed to consider the uncertainty of renewable power generation and take advantage of the most recent available information on forecasts. A sequence diagram for day-ahead and intraday operations was used for the purpose of illustration, and the cooperation of VPP and distribution network operator on congestion management was included.

The development of a cooperative solution for the provision of the congestion relief service by the VPP is the second and central contribution. The VPP can modify the schedules of selected units that have an effect on potential feeder overloads. The modification is motivated through participation in a flexibility market or bilateral agreement of VPP and DSO. The request of the DSO includes information on sensitivities that are calculated with the use of the AC power flow equations. The DSO provides these sensitivities to relate changes of branch flows to modifications of nodal power injections. Direct curtailment orders by the DSO are avoided. This way a dual service provision is achieved: Distributed wind and solar and other resources can participate in the market, while the network operator gets assistance through ancillary services. The methodology was validated using the CIGRE MV European benchmark, which is a representative distribution network for studying the integration of distributed energy resources. The results of the comparative analysis showed that at the time instants in which the congestion relief service was activated, the renewable power curtailment was prevented.

In sum, the aforementioned contributions support a shift of paradigm in power system operation. Apart from the transition of "generation follows load" towards "load follows generation" that a VPP can support through its pool of diverse units, it enables a move towards market-oriented solutions of network security. Compared with a situation where curtailments are ordered to maintain security, a solution based on agreements between network operator and VPP offers a mutual benefit in electricity market environments where a uniform marginal energy price is given.

## APPENDIX A

In this appendix, the equations for the dispatching of the units of the VPP are detailed. It is assumed for power curves not to vary inside the time step intervals considered. In the following equations, $\tau$ may either denote the day-ahead time step size $\tau_{\mathrm{da}}$ or the intraday time step size $\tau_{\mathrm{id}}$. The equations for the CHP units $i$ are the following:

$$C_{\mathrm{f,chp},i}(t_{\mathrm{h}}) = c_{\mathrm{NG}} \cdot \frac{1}{\eta_{\mathrm{chp},i}} \cdot P_{\mathrm{e,chp},i}(t_{\mathrm{h}}) \cdot \tau \tag{9}$$

$$P_{\mathrm{th,chp},i}(t_{\mathrm{h}}) = \lambda_{\mathrm{chp},i} \cdot P_{\mathrm{e,chp},i}(t_{\mathrm{h}}) \tag{10}$$

$$P_{\mathrm{e,chp},i,\min} \leq P_{\mathrm{e,chp},i}(t_{\mathrm{h}}) \leq P_{\mathrm{e,chp},i,\max} \tag{11}$$

Equation (9) gives the fuel cost $C_{\mathrm{f,chp}}(t_\mathrm{h})$ of each CHP unit $i$ for interval $\tau$ as a function of the natural gas price $c_\mathrm{NG}$, its electrical efficiency $\eta_\mathrm{chp}$ and its electrical power injection $P_\mathrm{e,chp}(t_\mathrm{h})$. Equation (10) gives the thermal power injection of the CHP $P_\mathrm{th,chp}(t_\mathrm{h})$ as a function of its electrical power injection $P_\mathrm{e,chp}(t_\mathrm{h})$ and the heat to electrical power ratio $\lambda_\mathrm{chp}$ of the unit. Equation (11) expresses the power limits of each CHP unit.

The storage units $i$ are modeled as follows:

$$C_{\mathrm{op,e,sto},i}(t_\mathrm{h}) = c_{\mathrm{op,e,sto},i} \cdot |P_{\mathrm{e,sto},i}(t_\mathrm{h})| \cdot \tau \tag{12}$$

$$E_{\mathrm{e,sto},i}(t_\mathrm{h}) =$$

$$\begin{cases} E_{\mathrm{e,sto},i}(t_\mathrm{h}-\tau) - \dfrac{P_{\mathrm{e,sto},i}(t_\mathrm{h})\cdot\tau}{\eta_{e,\mathrm{dis},i}}, P_{\mathrm{e,sto},i}(t_\mathrm{h}) > 0 \\ E_{\mathrm{e,sto},i}(t_\mathrm{h}-\tau) - P_{\mathrm{e,sto},i}(t_\mathrm{h})\cdot\tau\cdot\eta_{e,\mathrm{ch},i}, P_{\mathrm{e,sto},i}(t_\mathrm{h}) \le 0 \end{cases} \tag{13}$$

$$E_{\mathrm{e,sto},i,\min}(t_\mathrm{h}) \le E_{\mathrm{e,sto},i}(t_\mathrm{h}) \tag{14}$$

$$E_{\mathrm{e,sto},i}(t_\mathrm{h}) \le E_{\mathrm{e,sto},i,\max}(t_\mathrm{h}) \tag{15}$$

$$E_{\mathrm{th,sto},i}(t_\mathrm{h}) =$$

$$\begin{cases} E_{\mathrm{th,sto},i}(t_\mathrm{h}-\tau) - \dfrac{P_{\mathrm{th,sto},i}(t_\mathrm{h})\cdot\tau}{\eta_{\mathrm{th,dis},i}}, P_{\mathrm{th,sto},i}(t_\mathrm{h}) > 0 \\ E_{\mathrm{th,sto},i}(t_\mathrm{h}-\tau) - P_{\mathrm{th,sto},i}(t_\mathrm{h})\cdot\tau\cdot\eta_{\mathrm{th,ch},i}, P_{\mathrm{th,sto},i}(t_\mathrm{h}) \le 0 \end{cases} \tag{16}$$

$$E_{\mathrm{th,sto},i,\min}(t_\mathrm{h}) \le E_{\mathrm{th,sto},i}(t_\mathrm{h}) \tag{17}$$

$$E_{\mathrm{th,sto},i}(t_\mathrm{h}) \le E_{\mathrm{th,sto},i,\max}(t_\mathrm{h}) \tag{18}$$

Equation (12) gives the operational cost $C_{\mathrm{op,e,sto}}(t_\mathrm{h})$ of each electrical storage unit $i$ for interval $\tau$ as a function of the average operational cost $c_{\mathrm{op,e,sto}}$ per unit of energy, as described in [25], and the storage's power injection $P_{\mathrm{e,sto}}(t_\mathrm{h})$. The operational cost of the thermal storage was neglected. Equations (13) and (16) describe the energy level of each electrical or thermal storage unit. The energy level at each time instant depends on the energy level at the previous time step and the storage's power injection, considering the discharging or charging efficiency. At the beginning of the scheduling horizon, initial values $E_\mathrm{e,sto0}$ and $E_\mathrm{th,sto0}$ are assigned to the energy levels of the storage units. Equations (14), (15), (17), and (18) describe the energy capacity boundaries of each storage unit.

The active power imbalance exchanged in the intraday market is minimized by the VPP taking into consideration the following penalty cost:

$$C_\mathrm{pen,imb}(t_\mathrm{h}) = pf \cdot |P_\mathrm{imb,id}(t_\mathrm{h})| \cdot \tau \tag{19}$$

According to (19), the penalty cost for the imbalances is a function of the intraday imbalance $P_\mathrm{imb,id}(t_\mathrm{h})$ and a penalty factor $pf$ in EUR/MWh. In order to minimize the transactions of active power imbalance by the VPP in the intraday market, the value of the penalty factor $pf$ must be larger than the operational costs of the units of the VPP.

## Appendix B

The calculation of the sensitivities that are assigned to the VPP's resources to relax congestion over a congested branch $m$-$n$ is explained. Starting point of the calculation is the active power flow over a branch from nodes $m$ to $n$:

$$P_{\mathrm{f},mn} = |V_m|^2 g_{mn} - |V_m||V_n|[g_{mn}\cos(\theta_m-\theta_n) + b_{mn}\sin(\theta_m-\theta_n)] \tag{20}$$

A change in real power flow from $m$ to $n$ is given by [26]:

$$\Delta P_{\mathrm{f},mn} = \sum_{k=1}^{N} \frac{\vartheta P_{\mathrm{f},mn}}{\vartheta|V_k|}\Delta|V_k| + \sum_{k=1}^{N}\frac{\vartheta P_{\mathrm{f},mn}}{\vartheta\theta_k}\Delta\theta_k \tag{21}$$

where the counter $k$ from 1 to $N$ refers to the network's nodes. Equation (21) can be rewritten as follows:

$$\Delta P_{\mathrm{f},mn} = \left[\frac{\vartheta P_{\mathrm{f},mn}}{\vartheta\theta_1},\ldots,\frac{\vartheta P_{\mathrm{f},mn}}{\vartheta\theta_N}\frac{\vartheta P_{\mathrm{f},mn}}{\vartheta|V_1|},\ldots,\frac{\vartheta P_{\mathrm{f},mn}}{\vartheta|V_N|}\right] \begin{bmatrix}\Delta\theta_1\\ \cdots\\ \Delta\theta_N\\ \Delta|V_1|\\ \cdots\\ \Delta|V_N|\end{bmatrix} \tag{22}$$

The partial derivatives taken from (20) are shown in (23)-(26):

$$\frac{\vartheta P_{\mathrm{f},mn}}{\vartheta|V_m|} = 2|V_m|g_{mn} - |V_n|[g_{mn}\cos(\theta_m-\theta_n) + b_{mn}\sin(\theta_m-\theta_n)] \tag{23}$$

$$\frac{\vartheta P_{\mathrm{f},mn}}{\vartheta|V_n|} = -|V_m|[g_{mn}\cos(\theta_m-\theta_n) + b_{mn}\sin(\theta_m-\theta_n)] \tag{24}$$

$$\frac{\vartheta P_{\mathrm{f},mn}}{\vartheta\theta_m} = |V_m||V_n|g_{mn}\sin(\theta_m-\theta_n) - |V_m||V_n| \times b_{mn}\cos(\theta_m-\theta_n) \tag{25}$$

$$\frac{\vartheta P_{\mathrm{f},mn}}{\vartheta\theta_n} = -|V_m||V_n|g_{mn}\sin(\theta_m-\theta_n) + |V_m||V_n| \times b_{mn}\cos(\theta_m-\theta_n) \tag{26}$$

The vector of nodal angle and voltage changes on the right-hand-side of (22) also appears in the network power flow problem [26]. In the following equation, this vector is premultiplied by the Jacobian matrix $\boldsymbol{J}_{PQ,\theta V}$, and $[\Delta\boldsymbol{P},\Delta\boldsymbol{Q}]^\mathsf{T}$ is the vector of changes in nodal active and reactive power injections:

$$\begin{bmatrix}\Delta\boldsymbol{P}\\ \Delta\boldsymbol{Q}\end{bmatrix} = \boldsymbol{J}_{PQ,\theta V}\begin{bmatrix}\Delta\boldsymbol{\theta}\\ \Delta|\boldsymbol{V}|\end{bmatrix} \tag{27}$$

Making sure that $[\Delta\boldsymbol{\theta},\Delta|\boldsymbol{V}|]^\mathsf{T}$ does not cover the slack node and defining $\boldsymbol{J}_{\theta V,PQ} = \boldsymbol{J}_{PQ,\theta V}^{-1}$, (27) can be rearranged as follows:

$$\begin{bmatrix}\Delta\boldsymbol{\theta}\\ \Delta|\boldsymbol{V}|\end{bmatrix} = \boldsymbol{J}_{\theta V,PQ}\begin{bmatrix}\Delta\boldsymbol{P}\\ \Delta\boldsymbol{Q}\end{bmatrix} \tag{28}$$

Based on (28) and (22), the row vector $\boldsymbol{\alpha}_{mn}^\mathsf{T}$ with all the sensitivities of a power flow over branch $m$-$n$ toward changes of

nodal active and reactive power injections is as follows:

$$\boldsymbol{\alpha}_{mn}^{\mathsf{T}} = \left[ \frac{\vartheta P_{\mathrm{f},mn}}{\vartheta \theta_1}, \ldots, \frac{\vartheta P_{\mathrm{f},mn}}{\vartheta \theta_N}, \frac{\vartheta P_{\mathrm{f},mn}}{\vartheta |V_1|}, \ldots, \frac{\vartheta P_{\mathrm{f},mn}}{\vartheta |V_N|} \right] \boldsymbol{J}_{\theta V,PQ} \tag{29}$$

with

$$\boldsymbol{\alpha}_{mn}^{\mathsf{T}} = [\alpha_{\mathrm{P},mn,1}, \ldots, \alpha_{\mathrm{P},mn,N}, \alpha_{\mathrm{Q},mn,1}, \ldots, \alpha_{\mathrm{Q},mn,N}] \tag{30}$$

Equation (22) can then be rewritten as follows:

$$\Delta P_{\mathrm{f},mn} = \boldsymbol{\alpha}_{mn}^{\mathsf{T}} \left[\Delta P_1, \ldots, \Delta P_N, \Delta Q_1, \ldots, \Delta Q_N\right]^{\mathsf{T}} \tag{31}$$

In what follows, $\boldsymbol{a}_{mn}^{\mathsf{T}}$ is defined as a subvector of $\boldsymbol{\alpha}_{mn}^{\mathsf{T}}$ in order to only consider flow sensitivities with respect to power injections at nodes $i$ where VPP resources are present:

$$\boldsymbol{a}_{mn}^{\mathsf{T}} = [a_{\mathrm{P},mn,1}, \ldots, a_{\mathrm{P},mn,I}, a_{\mathrm{Q},mn,1}, \ldots, a_{\mathrm{Q},mn,I}] \tag{32}$$

where $I$ gives the number of VPP resources. Equation (31) then becomes for this special case:

$$\Delta P_{\mathrm{f},mn} = \boldsymbol{a}_{mn}^{\mathsf{T}} \big[\Delta P_{1,\mathrm{VPP}}, \ldots, \Delta P_{I,\mathrm{VPP}}, \Delta Q_{1,\mathrm{VPP}}, \ldots, \Delta Q_{I,\mathrm{VPP}}\big]^{\mathsf{T}} \tag{33}$$

## APPENDIX C

The selection of the data of the case study is explained. In particular, this concerns the selection of the DER data of the local network, as well as all the units within the VPP.

The left feeder of Fig. 5 represents an urban area. The number of households was firstly calculated for each bus, taking into consideration the MV and LV load data and profiles of [20]. The yearly average electricity demand of a single-family household in Germany is between 5000 kWh and 6000 kWh [27]. The residential load profile from [20] is assumed to concern the whole residential LV feeder. According to the aforementioned annual electricity demand, the daily peak of the residential feeder is estimated. Considering, then, the coincidence factor and the load data of [20], the number of households at each bus can be estimated. Moreover, the average annual heat load in Germany is 150 kWh/m$^2$ [28] with approximately 180 heating days per year. Based on this the daily heat energy demand is assessed.

It is assumed that consumers at buses 5, 6, 9, and 11 have a contract with the VPP. It is considered that 30% of the households of buses 5, 6, and 9 have a rooftop PV of 5 kW peak and a battery of maximum power output 5 kW, an energy efficiency of 95%, and power factors between 1 and 0.95 lagging or leading. It is assumed that the energy level of each storage unit at the end of the day is equal to its initial energy level. The total installed PV capacity in the VPP is 280 MW, 90 MW of which consists of rooftop PVs which are combined with electrical storage, as the ones already described. Furthermore, it is assumed that there is a local heat network supplying the VPP's consumers of buses 9 and 11. According to the number of households, the heat demand at these buses of the network is estimated, and it is also assumed that multiple CHP units of 100 kW electrical output, heat to electrical power ratio of 1.62, electrical efficiency of 35%, and power factor of 1 are used. Moreover, thermal storage units of maximum thermal power output of 100 kW and capacity of 200 kWh supplement the operation of the CHP units. The VPP controls more CHP units that serve further and similar local heat networks, as the ones of buses 9 and 11. The total installed CHP capacity within the VPP is 135 MW and is composed of small CHP units as the ones that were described. These CHP units are also combined with thermal storage of a total of 135 MW maximum thermal output for the whole VPP. The peak thermal load served by the VPP is 225 MW.

The units of the VPP on the local network cover only a small proportion of all the VPP's units. The total installed wind power generation capacity in the VPP is 400 MW. Furthermore, the VPP controls EV fleets in other areas with a total number of 5000 EVs. The EV charging strategy followed in this paper is based on [29], and it assumes that the EVs have a contract with the VPP. It allows the VPP to control the charging of the EVs at predefined periods of time. At the departure hour, an EV's battery is to be fully charged. The departure from home lies between 07:00 a.m. and 09:00 a.m. The return time varies between 08:00 p.m. and 10:00 p.m. The EVs are parked in residential areas and are assumed to charge with a maximum of 3 kW per hour. The battery energy capacity of each EV is considered to be 24 kWh with a charging efficiency of 90%. The VPP also has pumped-hydro units of total power output of 23 MW and storage capacity of 110 MWh. The peak of the VPP's electrical load is 280 MW.

Values for the average operational cost $c_{\mathrm{op,e,sto}}$ of storage units for each type of storage are taken from [25]. It is assumed that the modeled VPP has a contract for a natural gas price $c_{\mathrm{NG}}$ of 50 EUR/MWh.

## REFERENCES


[1] S. Wassermann, M. Reeg, and K. Nienhaus, "Current challenges of Germany's energy transition project and competing strategies of challengers and incumbents: The case of direct marketing of electricity from renewable energy sources," *Energy Policy*, vol. 76, pp. 66–75, Jan. 2015.

[2] K. Dietrich, J. M. Latorre, L. Olmos, and A. Ramos, "Modelling and assessing the impacts of self supply and market-revenue driven Virtual Power Plants," *Elect. Power Syst. Res.*, vol. 119, pp. 462–470, Feb. 2015.

[3] E. Mashhour and S. M. Moghaddas-Tafreshi, "Bidding strategy of virtual power plant for participating in energy and spinning reserve markets—Part I: Problem formulation," *IEEE Trans. Power Syst.*, vol. 26, no. 2, pp. 949–956, May 2011.

[4] M. R. Sarker, Y. Dvorkin, and M. A. Ortega-Vazquez, "Optimal participation of an electric vehicle aggregator in day-ahead energy and reserve markets," *IEEE Trans. Power Syst.*, vol. 31, no. 5, pp. 3506–3515, Sep. 2016.

[5] M. Giuntoli and D. Poli, "Optimized thermal and electrical scheduling of a large scale virtual power plant in the presence of energy storages," *IEEE Trans. Smart Grid*, vol. 4, no. 2, pp. 942–955, Jun. 2013.

[6] E. G. Kardakos, C. K. Simoglou, and A. G. Bakirtzis, "Optimal offering strategy of a virtual power plant: A stochastic bi-level approach," *IEEE Trans. Smart Grid*, vol. 7, no. 2, pp. 794–806, Mar. 2016.

[7] M. Rahimiyan and L. Baringo, "Strategic bidding for a virtual power plant in the day-ahead and real-time markets: A price-taker robust optimization approach," *IEEE Trans. Power Syst.*, vol. 31, no. 4, pp. 2676–2687, Jul. 2016.

[8] S. R. Dabbagh and M. K. Sheikh-El-Eslami, "Risk assessment of virtual power plants offering in energy and reserve markets," *IEEE Trans. Power Syst.*, vol. 31, no. 5, pp. 3572–3582, Sep. 2016.

[9] A. Mnatsakanyan and S. W. Kennedy, "A novel demand response model with an application for a virtual power plant," *IEEE Trans. Smart Grid*, vol. 6, no. 1, pp. 230–237, Jan. 2015.

[10] M. Heleno, M. A. Matos, and J. A. P. Lopes, "Availability and flexibility of loads for the provision of reserve," *IEEE Trans. Smart Grid*, vol. 6, no. 2, pp. 667–674, Mar. 2015.
[11] P. Moutis, P. S. Georgilakis, and N. D. Hatziargyriou, "Voltage regulation support along a distribution line by a virtual power plant based on a center of mass load modeling," *IEEE Trans. Smart Grid*, to be published.
[12] P. Moutis and N. D. Hatziargyriou, "Decision trees-aided active power reduction of a virtual power plant for power system over-frequency mitigation," *IEEE Trans. Ind. Informat.*, vol. 11, no. 1, pp. 251–261, Feb. 2015.
[13] L. Bird *et al.*, "Wind and solar energy curtailment: A review of international experience," *Renew. Sustain. Energy Rev.*, vol. 65, pp. 577–586, Nov. 2016.
[14] O. Sundstrom and C. Binding, "Flexible charging optimization for electric vehicles considering distribution grid constraints," *IEEE Trans. Smart Grid*, vol. 3, no. 1, pp. 26–37, Mar. 2012.
[15] J. Hu, S. You, M. Lind, and J. Ostergaard, "Coordinated charging of electric vehicles for congestion prevention in the distribution grid," *IEEE Trans. Smart Grid*, vol. 5, no. 2, pp. 703–711, Mar. 2014.
[16] A. Saint-Pierre and P. Mancarella, "Active distribution system management: A dual-horizon scheduling framework for DSO/TSO interface under uncertainty," *IEEE Trans. Smart Grid*, to be published.
[17] P. Meibom, R. Barth, B. Hasche, H. Brand, C. Weber, and M. O'Malley, "Stochastic optimization model to study the operational impacts of high wind penetrations in Ireland," *IEEE Trans. Power Syst.*, vol. 26, no. 3, pp. 1367–1379, Aug. 2011.
[18] E. A. Bakirtzis, P. N. Biskas, D. P. Labridis, and A. G. Bakirtzis, "Multiple time resolution unit commitment for short-term operations scheduling under high renewable penetration," *IEEE Trans. Power Syst.*, vol. 29, no. 1, pp. 149–159, Jan. 2014.
[19] H. Ding, Z. Hu, and Y. Song, "Rolling optimization of wind farm and energy storage system in electricity markets," *IEEE Trans. Power Syst.*, vol. 30, no. 5, pp. 2676–2684, Sep. 2015.
[20] "Benchmark systems for network integration of renewable and distributed energy resources," CIGRE Task Force C6.04.02, Tech Rep., 2014.
[21] A. J. Conejo, M. Carrion, and J. M. Morales, *Decision Making Under Uncertainty in Electricity Markets*. New York, NY, USA: Springer, 2010.
[22] Gurobi Optimization, Inc., "Gurobi optimizer reference manual," 2015. [Online]. Available: http://www.gurobi.com
[23] R. D. Zimmerman, C. E. Murillo-Sanchez, and R. J. Thomas, "MATPOWER: Steady-state operations, planning and analysis tools for power systems research and education," *IEEE Trans. Power Syst.*, vol. 26, no. 1, pp. 12–19, Feb. 2011.
[24] X. Y. Ma, Y. Z. Sun, and H. L. Fang, "Scenario generation of wind power based on statistical uncertainty and variability," *IEEE Trans. Sustain. Energy*, vol. 4, no. 4, pp. 894–904, Oct. 2013.
[25] B. Zakeri and S. Syri, "Electrical energy storage systems: A comparative life cycle cost analysis," *Renew. Sustain. Energy Rev.*, vol. 42, pp. 569–596, Feb. 2015.
[26] A. J. Wood and B. F. Wollenberg, *Power Generation Operation and Control*. New York, NY, USA: Wiley, 1996.
[27] M. Hayn, V. Bertsch, and W. Fichtner, " Electricity load profiles in Europe: The importance of household segmentation," *Energy Res. Social Sci.*, vol. 3, pp. 30–45, Sep. 2014.
[28] V. Badescu and B. Sicre, "Renewable energy for passive house heating: Part I. Building description," *Energy Build.*, vol. 35, pp. 1077–1084, Dec. 2003.
[29] R. J. Bessa, M. A. Matos, F. J. Soares, and J. A. P. Lopes, "Optimized bidding of a EV aggregation agent in the electricity market," *IEEE Trans. Smart Grid*, vol. 3, no. 1, pp. 443–452, Mar. 2012.

**Despina Koraki** received the Diploma in electrical engineering from the School of Electrical and Computer Engineering, National Technical University of Athens, Greece, in 2012. Since February 2013, she has been working as a Research Assistant at the Technische Universität Berlin, Germany. Her research interests include the integration of renewable resources in power systems and energy markets and the provision of services to system operators through virtual power plants.

**Kai Strunz** has been a Professor of sustainable electric networks and sources of energy at Technische Universität Berlin, Germany, since 2007.

Dr. Strunz is the Chair of the IEEE PES Subcommittee on Distributed Energy Resources. He has received the IEEE PES Prize Paper Award 2015 and the IEEE Journal of Emerging and Selected Topics in Power Electronics First Prize Paper Award 2015. In 2012, he was the General and Technical Program Chair of the IEEE PES Innovative Smart Grid Technologies Europe 2012 in Berlin.